



Ab initio potential energy surface and quantum scattering studies of Li^+ with N_2 : comparison with experiments at $E_{\text{c.m.}} = 2.47$ eV and 3.64 eV

ABHINAV KUMAR and SANJAY KUMAR*

Department of Chemistry, Indian Institute of Technology Madras, Chennai, Tamil Nadu 600 036, India
E-mail: sanjay@iitm.ac.in

MS received 2 August 2018; revised 4 September 2018; accepted 5 September 2018; published online 30 October 2018

Abstract. A new ground electronic state potential energy surface of $\text{Li}^+ + \text{N}_2$ system is presented in the Jacobi scattering coordinates at MRCI level of accuracy employing the augmented correlation-consistent polarized valence quadrupole zeta (aug-cc-pVQZ) basis set. An analytic fit of the computed *ab initio* surface has also been obtained. The surface has a global minimum for the collinear geometry at the internuclear distance of N_2 , $r = 2.078a_0$, and the distance between Li^+ and N_2 , $R = 4.96a_0$. Quantum dynamics studies have been performed within the vibrational close coupling-rotational infinite-order sudden approximation at $E_{\text{c.m.}} = 3.64$ eV, and the collision attributes have been analyzed. The computed total differential cross-sections are found in quantitative agreement with those available from the experiments at $E_{\text{c.m.}} = 3.64$ eV. The other dynamic attributes such as angle dependent opacities and integral cross-sections are also reported. Preliminary rigid-rotor and vibrational-rotational coupled-state calculations at $E_{\text{c.m.}} = 2.47$ eV also support the experimental observation that the system exhibits a large number of rotational excitations in the vibrational manifold $v = 0$.

Keywords. Potential energy surface; quantum dynamics; vibrational-rotational excitations.

1. Introduction

Ion-molecule collisions leading to vibrational-rotational and electronic (charge transfer) excitations are important in several areas of Chemical Physics, Astrophysics and Atmospheric Chemistry.^{1,2} Collisions of H^+ ion with diatomic and polyatomic molecules have been studied extensively both by experiments and theory.² But, collisions with relatively larger Li^+ ion with molecules have not received much attention although the experimental data on its collisions with N_2 and CO became available as early as 1976.³ Li^+ ion has a closed-shell electronic structure of He but possesses a positive charge. Several experimental and theoretical studies are available for collisions of diatoms with He, Ne and Ar. For example, see references⁴⁻⁶ and references therein. The interactions of Li^+ with molecules is of particular interest since they are dominated by both short-range valence and long-range interactions. Being a four-electron system, the $\text{Li}^+ + \text{H}_2$ system² has been investigated relatively more than the $\text{Li}^+ + \text{N}_2$ and $\text{Li}^+ + \text{CO}$ systems. Vibrational and/or rotational

excitations of N_2 and CO on collisions with Li^+ have been studied experimentally at (i) low collision^{3,7,8} ($E_{\text{coll}} < 20$ eV), (ii) moderate collision energies^{9,10} ($E_{\text{coll}} \sim 70$ –350 eV) and high collision energies¹¹ ($E_{\text{coll}} > 500$ eV).

The present study is focused on the inelastic vibrational-rotational excitations in $\text{Li}^+ + \text{N}_2$ system at low collision energies. In the asymptotic limit, the charge transfer channel $\text{Li} + \text{N}_2^+$ is endoergic ($\Delta E \approx 10.2$ eV) in comparison to entrance $\text{Li}^+ + \text{N}_2$ channel, and therefore at low energies, one expects that inelastic vibrational-rotational excitations would occur involving only the ground electronic state (GS) of the system.

Measurements of inelastic scattering of Li^+ with N_2 (and CO) were carried out by Böttner *et al.*,³ using time-of-flight spectra of scattered Li^+ at collision energy (in the center of mass frame) $E_{\text{c.m.}} = 4.23$ eV and 7.07 eV over a wide range of scattering angles, $\theta_{\text{c.m.}}$. Some additional data of time-of-flight measurements⁷ also became available at $E_{\text{c.m.}} = 8.4$ eV and 16.8 eV for $\theta_{\text{c.m.}}$ in the range of 30°–120°. The measured spectra showed two well-resolved peaks identified with vibrational excitations ($v = 0 \rightarrow v' = 0$ and $v = 0 \rightarrow v' = 1$) and their broadening was identified with large number

*For correspondence

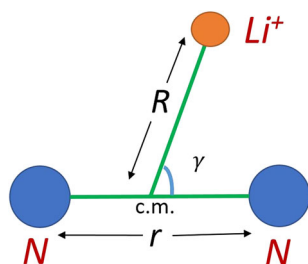


Figure 1. Jacobi coordinates. r : internuclear distance of N_2 ; R : distance of Li^+ atom from the c.m. of N_2 ; γ : angle between r and R .

of rotational excitations ($j' \approx 30$) in each vibrational manifold.

On the theoretical side, the information on the potential energy surface (PES) was first provided by Staemmler¹² at the self-consistent field (SCF) level of accuracy in the Jacobi scattering coordinates (Figure 1). The dependence of internuclear distance ($1.8a_0 \leq r \leq 2.3a_0$) of N_2 was analyzed only for collinear ($\gamma = 0^\circ$) and perpendicular ($\gamma = 90^\circ$) approaches of Li^+ . The rigid-rotor (RR) PES was obtained as a function of R ($= 2.0\text{--}20a_0$) and γ ($= 0^\circ, 30^\circ, 60^\circ, 90^\circ$), and a fit was obtained in terms of Legendre expansion. The errors associated with the PES and the computed values of polarizabilities and quadrupole moments were estimated to be within 20 per cent.

Staemmler's *ab initio* points were used in subsequent theoretical studies. Thomas¹³ obtained a 48-parameter analytical fit (within 14 per cent error) where γ -dependence was obtained in terms of Legendre expansion and r -dependence was taken in terms of Taylor series expansion around $r = r_{\text{eq}}$ up to quadratic terms. His quasi-classical trajectory (QCT) calculations were found in overall qualitative agreement but lacked agreement with experiments for rotational distribution. Almost at the same time, Poppe and Böttner¹⁴ obtained a similar type of fit using the combination of least square and cubic spline fits and carried out QCT calculations. Their results were in overall good qualitative agreement and they attributed the differences observed between the experiment and theory to the inaccuracy in the PES. Subsequently, Billing¹⁵ obtained an analytic fit using 95 *ab initio* points with an error estimate within 6 per cent and carried out semi-classical calculations describing the vibrational motion quantum mechanically and translational and rotational motions classically. He obtained narrower rotational distributions in comparison with those of experiments. Pfeffer and Secrest¹⁶ obtained another analytic fit on similar lines with similar

percentage error but they believed that their fit provided the better angular dependency. They studied vibrational-rotational excitations using quantum mechanical vibrational close coupling-rotational infinite-order sudden approximation (VCC-RIOSAs) and carefully analyzed the computed differential cross sections (DCS) in the experimental range ($30^\circ\text{--}60^\circ$) and found the distribution of rotational excitations in disagreement with those observed in the experiments.

Various theoretical studies predicting the thermodynamic and structural properties of $\text{Li}^+ + \text{N}_2$ have also been reported¹⁷ which supplement data only around the stationary points on the PES and therefore provided limited information on the full PES. There have also been attempts¹⁸ to construct the spherically averaged potential ($V_0(R)$ term in the Legendre polynomial expansion of the RR potential) through the measurements of total (elastic) cross sections in high collision energy range.

The SCF PES of Staemmler¹² lacked accuracy in terms of electron correlation. Therefore, Grice *et al.*,¹⁹ computed a new RR PES employing the Hartree-Fock (HF) and Møller-Plesset (MP) levels of theories and examined the improvement achieved in terms of enlargement of basis set and retrieval of electron correlation. They computed the RR PES for $R = 1.0\text{--}12 \text{ \AA}$, $\gamma = 0^\circ, 22.5^\circ, 45^\circ$ and 90° . Subsequently, a more recent *ab initio* study was undertaken by Falcetta and Siska²⁰ to compute the RR PES for $\text{He}^+/\text{Li}^+ + \text{N}_2$ systems for $R = 3.0\text{--}20.0a_0$ and $\gamma = 0^\circ, 45^\circ$ and 90° . To describe the long-range RR potential they also computed various multipolar terms (polarizabilities, quadrupole moments, etc.) with high accuracy and obtained an analytic fit. Recently, Bulanin *et al.*,²¹ computed the PES around the van der Waals' interaction well and the energetically low-lying bound states of $[\text{LiN}_2]^+$ complex.

To the best of our knowledge, an accurate full PES incorporating the dependence of the vibrational coordinate and angular approaches over a fine grid is still lacking for the $\text{Li}^+ + \text{N}_2$ system. Therefore, we have computed the full PES in the Jacobi coordinates and also obtained an analytic fit in order to carry out quantum dynamics of vibrational-rotational excitation so that the results can be compared with the existing experimental data meaningfully. Computational details of the PES are presented in section 2 and its various characteristics are examined there. A preliminary quantum dynamics study has been carried out within the VCC-RIOSAs framework at $E_{\text{c.m.}} = 3.64 \text{ eV}$ and RR and vibrational-rotational coupled-state calculations at $E_{\text{c.m.}} = 2.47 \text{ eV}$. The details are presented in section 3, and a summary with the conclusions is given in section 4.

2. Computational details

2.1 *Ab initio* calculations

All the calculations presented here were performed in the Jacobi coordinates (Figure 1) on the following grid points: $r = 1.5\text{--}3.3$ (0.1); $R = 1.9\text{--}3.1$ (0.2), $3.1\text{--}5.6$ (0.1), $5.6\text{--}7.2$ (0.2), $7.2\text{--}10.2$ (0.5), $10.2\text{--}14.2$ (1.0); $\gamma = 0^\circ\text{--}90^\circ$ (15°). R and r are in atomic units and the number in parenthesis indicates the interval in the stated range. The total number of computed *ab initio* points were approximately 6500. Calculations were performed in C_{2v} point group for collinear and perpendicular approaches, and in C_s point group for other approaches.

In the present calculations, we employed an augmented correlation-consistent polarized valence quadrupole zeta (aug-cc-pVQZ) basis ((13s7p4d3f2g)/[6s5p4d3f2g]) of Duning.²² Falcetta and Siska²⁰ had used a truncated aug-cc-pVQZ basis set²³ yielding (13s7p4d3f2g)/[6s5p4d2f] basis. For each point, a HF calculation was performed, followed by a complete active space self-consistent field²⁴ (CASSCF) calculation. The resulting molecular orbitals (MOs) were used as a reference space to construct multi-reference single and double excitations. Self-consistent field internally contracted multi-reference configuration interaction²⁵ (SCF-icMRCI) calculations were performed using MOLPRO 2010.1²⁶ program. The lowest three MOs in energy were kept as core orbitals and next 12 MOs ($6A_1, 3B_1, 3B_2$ for $\gamma = 0^\circ$; $5A_1, 2B_1, 4B_2, 1A_2$ for $\gamma = 90^\circ$; $9A', 3A''$ for $0^\circ < \gamma < 90^\circ$) were treated as valence orbitals. Typically, the wavefunction consisted of 43194 configuration state functions (CSFs) with 157464 Slater determinants. The MRCI calculations were performed with a reference space of 15549 configurations. The numbers of internal configurations N , $N-1$ and $N-2$ were 58278, 43252 and 28314, respectively. The total number of contracted configurations was 11621739 with 43194 internal, 10642536 singly external and 936009 doubly external configurations. The threshold value for the selection of CSFs was kept at 3.2×10^{-5} a.u. For example, the following energy values were obtained for $r = 2.0812a_0$, $R = 2.7a_0$ and $\gamma = 0^\circ$: $E(\text{HF}) = -114.9683$ a.u., $E(\text{CASSCF}) = -115.5687$ a.u. and $E(\text{MRCI}) = -115.77$ a.u.

Before we present the results on PES, it would be important to ascertain the quality of computation by comparing the structural and electric properties of N_2 with those obtained from the experiments and earlier theoretical calculations. Table 1 lists the various calculated^{12,19,20} and experimental data.^{27–29} The SCF calculations of staemmler¹² yielded relatively lower values for all the properties. Grice *et al.*,¹⁹ computed them at the HF level and also incorporated electron correlation through perturbative MP calculations by enlarging the basis set. Their r_{eq} values were found to be approximately shorter by $0.05a_0$ ($\sim 2.024a_0$) in comparison to the experimental value and remained almost the same in going from the HF to MP2 levels of calculations, and so was the case for quadrupole moment ($Q \sim -1.26$ a.u.). However, the values for polarizabilities did show some improvement in comparison with those of experiments. Falcetta and Siska²⁰ had used the experimental value for $r = r_{\text{eq}}$ (i.e., $2.074a_0$), and their values for Q and α 's are in close agreement with those of experiments. The computed value of Bulanin *et al.*,²¹ for r_{eq} was $2.066a_0$ at CCSD/cc-pVQZ level of theory. Their computed values for other electric properties are not available and therefore they are not listed in Table 1. We used Gaussian 09 program suite³⁰ to compute parallel (α_{\parallel}) and perpendicular (α_{\perp}) polarizability components at configuration interaction with all single and double substitutions (CISD) level of accuracy. Our optimized values of r_{eq} and polarizability components are also in close agreement with those of Falcetta and Siska and the experiments. Considering the error bar in the experiment, the quadrupole moment is also well reproduced in the present calculations.

Falcetta and Siska²⁰ carried out systematic investigations of the basis set superposition error (BSSE) using the counterpoise method,³¹ and their RR PES was obtained using the BSSE corrected data points. They observed that BSSE corrections were small compared to the net interaction energy of $Li^+ + N_2$; For example, for $\gamma = 0^\circ$ their BSSE corrections were 0.02 kcal/mol (0.0009 eV) at $R = 10.0a_0$, 0.16 kcal/mol (0.007 eV) at $R = 5.0a_0$ and 0.57 kcal/mol (0.02 eV) at $R = 3.0a_0$. In the present calculations, the BSSE corrections were found to be in the similar range. In view of small magnitudes of BSSE corrections, particularly in the well and long-range

Table 1. Structural and electronic properties of N_2 . All values are in atomic units.

Theory/basis	r_e	Q	α_{\parallel}	α_{\perp}
Staemmler ¹² HF/(9s4p+2d)	2.018	−0.94	13.46	9.73
Grice <i>et al.</i> ¹⁹ HF/6-311+G(df)	2.018	−1.26	14.68	7.01
MP4SDTQ/6-311+G(2df)	—	—	14.13	8.57
Falcetta and Siska ²⁰ MRCI/(13s7p4d2f3d)/[6s5p4d2f]	—	−1.067	14.62	9.9
Present calculations MRCI/aug-cc-pVQZ	2.08	−1.124	14.712	9.96
Experiment	2.074 ²⁷	−1.09 ± 0.05 ²⁸	14.81 ²⁹	10.2 ²⁹

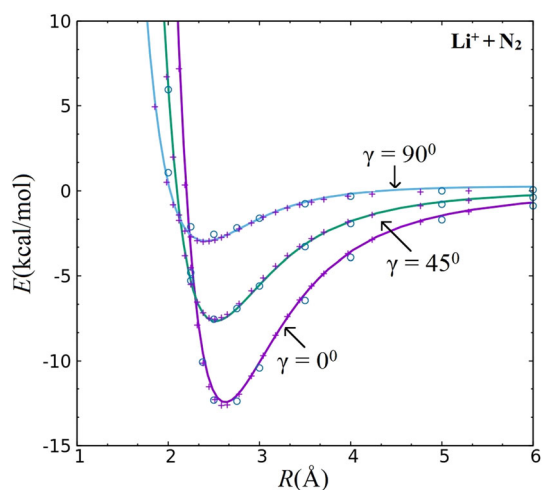


Figure 2. Computed potential energy curves as a function of R with $r = r_{\text{eq}}$ (see the text) for $\gamma = 0^\circ$, 45° and 90° . The *ab initio* data points of Falcetta and Siska²⁰ and Grice *et al.*,¹⁹ are shown with ‘+’ and ‘o’ symbols, respectively. The present calculations are shown as solid curves.

regions, and scattering dynamics for collision energy $E_{\text{c.m.}} \geq 2.47$ eV, we believe that non-inclusion of BSSE corrections will not result into a significant error. Therefore, in the present study, we report the computed *ab initio* energies without the BSSE correction. For reference, we report the following computed energies: $E(\text{Li}^+; ^1\text{S}) = -7.2526$ a.u. and $E(\text{N}_2; ^1\Sigma_g^+, r_{\text{eq}} = 2.081a_0) = -109.392$ a.u.

In order to compare our results with those of earlier theoretical calculations, we have plotted the RR potential energy curves (PEC) for $\gamma = 0^\circ$, 45° and 90° as a function of R in Figure 2. The present results are shown for our optimized value of $r_{\text{eq}} = 2.0812a_0$. Falcetta and Siska²⁰ had used experimental value of $r_{\text{eq}} = 2.074a_0$ while r_{eq} used by Grice *et al.*,¹⁹ was $2.024a_0$. The corresponding results are reproduced in Figure 2. It can be seen that the present results (solid lines) are in close agreement with both the results, more so with those of Falcetta and Siska.²⁰ The $\text{Li}^+ + \text{N}_2$ interaction well is found to be the deepest in collinear geometry ($\gamma = 0^\circ$). Therefore, it would be worthwhile to compare its characteristics with those of earlier calculations. In Table 2, its various parameters have been compared. Once again, the present calculations are in close agreement with Falcetta and Siska.

It would also be important to examine the well characteristics of the spherically averaged term, $V_0(R)$ of the Legendre expansion of the RR interaction potential defined as

$$V(R, r = r_{\text{eq}}, \gamma) = \sum_{\lambda=0} V_{\lambda}(R, r = r_{\text{eq}}) P_{\lambda}(\cos \gamma) \quad (1)$$

where P_{λ} 's are the Legendre polynomials. The various parameters are summarized in Table 3 along with earlier theoretical^{12, 17a, 19, 20} and experimental¹¹ results. Gislason *et al.*,¹¹ had deduced these values from their total cross-section measurements for Li^+ ions scattered from N_2 in the

Table 2. Characteristics of computed $\text{Li}^+ + \text{N}_2$ interaction potential well in collinear geometry ($\gamma = 0^\circ$). R_0 defines the R at which the PEC crosses the zero-energy line in the repulsive region.

Reference	r/a_0	R/a_0	R_0/a_0	$D_e/\text{Kcal/mol}$
Staemmler ¹²	2.067	4.964	4.157	13.03
Waldman <i>et al.</i> ^{17a}	–	4.648	3.893	14.2
Dixon <i>et al.</i> ^{17b}	2.018	4.972	–	11.36
Grice <i>et al.</i> ¹⁹	2.016	4.947	4.123	12.84
Falcetta and Siska ²⁰	2.074	4.932	4.133	12.648
Present calculations	2.08	4.962	4.157	12.443

Table 3. Well characteristics of spherically averaged $V_0(R)$ potential for $\text{Li}^+ + \text{N}_2$ complex. For definition, see the text. R_0 defines the R at which the PEC crosses the zero-energy line in the repulsive region.

Reference	R_e/a_0	R_0/a_0	$D_e/\text{kcal/mol}$
Staemmler ¹²	4.752	3.921	7.516
Waldman <i>et al.</i> ^{17a}	4.612	3.856	5.13
Gislason <i>et al.</i> ¹¹	4.802	3.932	7.32
Grice <i>et al.</i> ¹⁹	4.817	3.977	5.89
Falcetta and Siska ²⁰	4.732	3.952	6.015
Present calculations	4.767	3.977	6.014

range $E\theta_{\text{lab}} = 5\text{--}1000$ eVdeg. There has been an uncertainty regarding the estimate of the well depth as it varied in both theoretical and experimental estimates. One can see again that the present calculations are in close agreement with those of Falcetta and Siska.²⁰

2.2 Analytic fit of the PES

The computed PES exhibits a smooth behavior as a function of R , r and γ . One of the general ways of obtaining a fit of *ab initio* points is to expand the potential terms in Legendre polynomials

$$V(R, r, \gamma) = \sum_{\lambda=0} V_{\lambda}(R, r) P_{\lambda}(\cos \gamma) \quad (2)$$

The coefficients V_{λ} are dependent on both R and r . Following our earlier experience with the fitting of PES for the $\text{H}^+ + \text{CO}$ system³² we have tried the similar fitting here, that is,

$$V(R, r, \cos \gamma) = \sum_{i=1}^7 \sum_{j=1}^{7-i} \sum_{k=1}^7 C_{ijk} \left(\frac{1}{R}\right)^i \left(\frac{1}{r}\right)^j (\cos \gamma)^k \quad (3)$$

which yielded 196 coefficients to be determined by the standard least-square method. The following ranges were used to obtain the fitting: $1.5a_0 \leq r \leq 3.3a_0$; $1.9a_0 \leq R \leq 14.2a_0$ and $0^\circ \leq \gamma \leq 90^\circ$ with a root mean square error of 0.2266×10^{-3} a.u. (0.00616 eV). The values of the

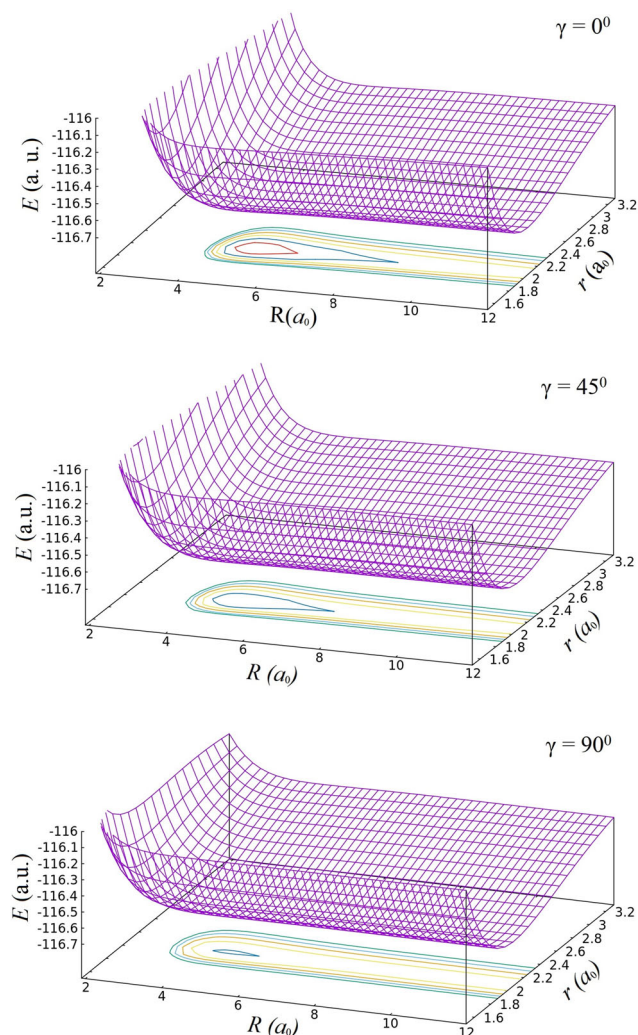


Figure 3. PESs and contour plots of $\text{Li}^+ + \text{N}_2$ complex as a function of r and R for three different orientations, $\gamma = 0^\circ$, 45° and 90° .

coefficients and the FORTRAN code of the *ab initio* fitting are available upon request.

Figure 3 displays the PESs and the contour plots as a function of R and r for $\gamma = 0^\circ$, 45° and 90° . The topology of these PESs is almost identical except that the depth of the interaction well becomes successively less in going from $\gamma = 0^\circ$ to $\gamma = 90^\circ$. Interestingly, an analysis of r_{eq} , R_{eq} values corresponding to the bottom of the interaction well reveals that r_{eq} does not show any significant change and remains almost equal to the value of r_{eq} of N_2 and that R_{eq} varies from $4.96a_0$ to $4.55a_0$ in going from the collinear to the perpendicular approaches.

2.3 Long-range interactions

For homonuclear N_2 , the odd multiple moments such as dipole, octupole, etc., have zero values and only the even multipole moments such as quadrupole, hexadecapole, etc., will survive. Falcetta and Siska²⁰ had computed values for

Table 4. Coefficients used in the fitting of long-range potential. See eqs. (4) and (5). All values are in atomic units.

Property	a_0	a_1	a_2	a_3	a_4
Q	-1.125	0.989	0.100	-0.113	-0.110
α_0^d	11.561	6.033	0.459	1.660	-1.894
α_2^d	4.791	6.892	0.479	6.679	-5.942

quadrupole, hexadecapole and tetrahexacontapole values at $r_{\text{eq}} = 2.074a_0$. In the present study, we consider only the quadrupole and the polarizability components to be the contributing factors for long-range interaction potential since we believe that other components would have negligible contributions in view of collision dynamics for energies, $E_{\text{c.m.}} \geq 2.47$ eV. We obtained the asymptotic potential (V_{asympt}) using eqs. (4), (5) and (6). We used the same aug-cc-pVQZ basis set to compute these properties as a function of r at MRCI level of theory and fitted them using the polynomial (eq. 5) as a function of r . As mentioned above, r_{eq} taken in the present calculations is $2.0812a_0$. The coefficients were obtained using the least-square method and they are given in Table 4. The root mean square errors for the fits of Q, α_{\parallel} and α_{\perp} were 0.00029 a.u., 0.00022 a.u., and 0.00276 a.u. respectively.

$$V_{\text{asympt}} \sim \frac{Q(r)}{R^3} P_2(\cos \gamma) - \frac{\alpha_0(r)}{2R^4} - \frac{\alpha_2(r)}{2R^4} P_2(\cos \gamma) + O(P_3) \quad (4)$$

$$f(r) = a_0 + a_1(r - r_{\text{eq}}) + a_2(r - r_{\text{eq}})^2 + a_3(r - r_{\text{eq}})^3 + a_4(r - r_{\text{eq}})^4 \quad (5)$$

$$\alpha_d^0 = \frac{1}{3} (\alpha_{\parallel} + 2\alpha_{\perp}) \text{ and } \alpha_d^2 = \frac{2}{3} (\alpha_{\parallel} - \alpha_{\perp}) \quad (6)$$

The *ab initio* PES and the long-range PES were joined smoothly at $R = 14.2a_0$.

2.4 Vibrational coupling matrix elements

Before we present the results of dynamics calculations it would be worthwhile to analyze the strengths of vibrational coupling matrix elements (VCMEs) defined by

$$V_{vv'}(R, \gamma) = \langle \phi_v(r) | V_{\text{in}}(R, r, \gamma) | \phi_{v'}(r) \rangle \quad (7)$$

where ϕ_v and $\phi_{v'}$ represent the initial and final vibrational state wavefunctions of N_2 , and $V_{\text{in}}(R, r, \gamma)$ ($V_{\text{total}}(R, r, \gamma) - V_{\text{total}}(R = 100a_0, r, \gamma)$) denotes the interaction potential which goes to zero value at asymptotic separations, $R = 100a_0$. The vibrational wave functions $\phi_v(r)$ were obtained numerically using the Le Roy code³³ and N_2 PEC. The strengths of VCMEs is related to the probability of vibrational excitation. The VCMEs as a function of R for $\gamma = 0^\circ$, 45° and 90° are shown in Figure 4. They show a smooth behavior and there is a relatively deep potential well for V_{00} for all angles between 0° and 90° indicating a strong coupling in

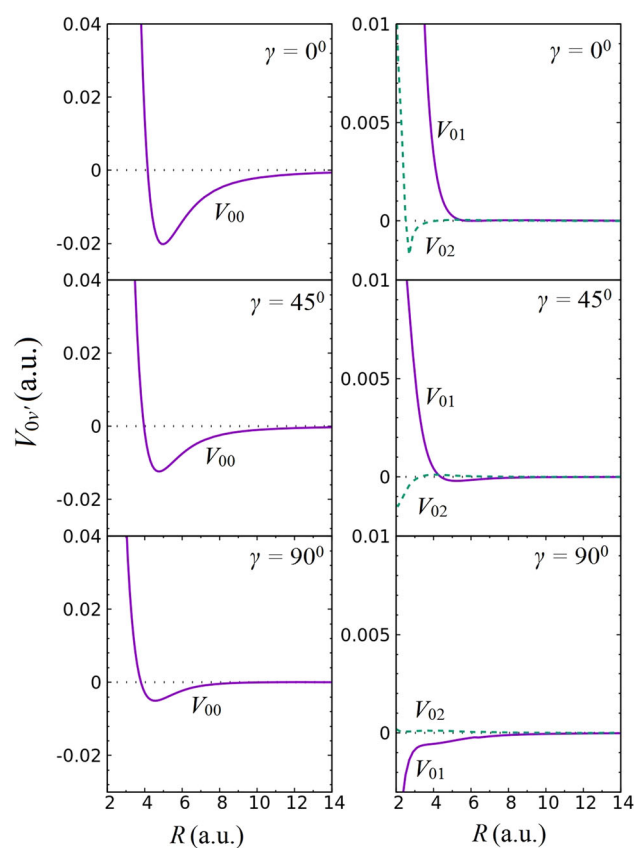


Figure 4. Vibrational coupling matrix elements defined in eq. (7) as a function of R for $\gamma = 0^\circ, 45^\circ$ and 90° . Left panel: V_{00} ; Right panel: V_{01} and V_{02} . See the text.

the vibrationally elastic channel. The coupling elements for inelastic channels (V_{01} and V_{02}) are relatively much weaker than V_{00} and $V_{01} > V_{02}$. Also, they are significantly small for $R \geq 5a_0$ indicating weak vibrational inelasticity in the system as it was observed in the experiments.³

3. Results and Discussion

3.1 Quantum dynamics within VCC-RIOSIA approximation

The rotational states of N_2 are much more densely packed as compared to that of H_2 . Therefore, as collision energy increases the treatment of quantum dynamics in the close-coupling formalism successively becomes computationally prohibitive. Hence, it would be worthwhile to invoke the VCC-RIOSIA approximation. The theory of VCC-RIOSIA has been well discussed and well documented in the literature. For example, see references^{34–36} and references therein. Therefore, we summarize only the essential details here. The first approximation is the decoupling of rotational and orbital angular momenta, which can be valid when the

interaction (collision) time of the projectile is much shorter than the rotational period of the diatom. The second approximation is based on the fact that rotational states are closely packed so that differences between rotational energy levels are small compared to the translational energy of the collision. Both of these approximations, known as the centrifugal sudden and energy sudden approximations, could be well justified at relatively higher collision energies. The VCC-RIOSIA approximation leads to a drastic reduction in the coupled-channel equations wherein one essentially solves the vibrational–translational motions quantum mechanically by decoupling the angular momenta for different fixed values of γ . Successful applications of VCC-RIOSIA have been reported for energies as low as $E_{c.m.} = 3.7$ eV for the $H^+ + H_2$ system.³⁷ The experiments of Böttner *et al.*,³ reported total vibrational excitation differential cross sections for $E_{c.m.} = 3.64$ eV ($E_{lab} = 4.5$ eV) and $E_{c.m.} = 2.47$ eV ($E_{lab} = 3.5$ eV). They also published some data on the distribution of rotationally excited states in $v = 0$ and 1 manifolds for three different scattering angles for $E_{c.m.} = 4.23$ eV and 7.07 eV. Therefore, in the present study we carried out VCC-RIOSIA calculations at $E_{c.m.} = 3.64$ eV and compared them with those of experiments. It is important to note here that Pfeffer and Secret¹⁶ had also studied vibrational–rotational excitations in the system within VCC-RIOSIA approximation at $E_{c.m.} = 4.23$ eV. Their calculations could show low vibrational inelasticity, but their computed rotational distributions for DCSs at $\theta_{c.m.} = 37.1^\circ, 43.2^\circ, 49.2^\circ$ were found to be narrower than those of experiments. In the present study, we focus on the DCS for total rotationally-summed vibrational excitations and compare them with that available from experiments at $E_{c.m.} = 3.64$ eV.

Since the sudden S-matrix elements in ion–molecule system^{16,35} are known to show a strong γ -dependence, particularly at smaller values of orbital angular momentum (l), it was useful to expand their angular dependence in terms of Legendre expansion. Accordingly, the T -matrix elements were expanded as,

$$T_{vv'}^{\bar{j}l} = \sum_{\lambda} A_{\lambda}^l(\bar{j}v \rightarrow v') P_{\lambda}(\cos \gamma) \quad (8)$$

where \bar{j} is the initial rotational state (usually set as zero), v and v' are the initial and final vibrational states, and the transition indicates the excitation from an initial state ($\bar{j}v$) to a rotationally-summed vibrational state (v'). The working formula for the rotationally-summed DCS and integral cross sections (ICS) are given in terms of $A_{\lambda}^l(\bar{j}v \rightarrow v')$ as³⁵

$$\frac{d\sigma}{d\omega}(\bar{j}v \rightarrow v') = \sum_{\lambda} (2\lambda + 1)^{-1} \frac{d\sigma^{\lambda}}{d\omega}(\bar{j}v \rightarrow v') \quad (9)$$

where

$$\begin{aligned} \frac{d\sigma^{\lambda}}{d\omega}(\bar{j}v \rightarrow v') \\ = \left(\frac{1}{4k_{jv}^2} \right) \left| \sum_l (2l + 1) P_l(\cos \theta_{cm}) A_{\lambda}^l(\bar{j}v \rightarrow v') \right|^2 \end{aligned} \quad (10)$$

$\theta_{c.m.}$ is the scattering angle in the center of mass frame, and k_{jv} is the wave vector

$$k_{jv} = \frac{\sqrt{2\mu(E - \varepsilon_{jv})}}{\hbar} \quad (11)$$

ε_{jv} denotes the vibrational–rotational energy of the diatom, and E is the total energy. The integral cross sections for rotationally-summed vibrational excitations were obtained as

$$\sigma(\bar{j}v \rightarrow v') = \sum_{\lambda} (2\lambda + 1)^{-1} \sigma^{\lambda}(\bar{j}v \rightarrow v') \quad (12)$$

With,

$$\sigma^{\lambda}(\bar{j}v \rightarrow v') = \left(\frac{\pi}{k_{jv}^2} \right) \sum_l (2l + 1) |A_{\lambda}^l(\bar{j}v \rightarrow v')|^2 \quad (13)$$

In the present calculations, the radial vibrational coupled-channel equations were integrated using the sixth-order Numerov method (from initial R_i values well below the classical turning points up to final $R_f = 100a_0$) for 7 equally spaced γ -values between 0° and 90° , for each partial wave (l). Ten vibrational levels of N_2 were included and the maximum value of l_{max} was 4050 at $E_{c.m.} = 3.64$ eV for reaching the numerical convergence for elastic and inelastic vibrational excitations up to $v' = 3$.

3.2 Computed dynamical attributes

It would be worthwhile to examine the characteristics of angle-dependent opacity functions (partial cross sections) as they provide useful insight into the collision dynamics and they are defined as

$$\sigma^l(\bar{j}v \rightarrow v'; \gamma) = \left(\frac{\pi}{k_{jv}^2} \right) (2l + 1) |T_{vv'}^l(\gamma)|^2 \quad (14)$$

The opacities are shown in Figure 5 for (a) $v = 0 \rightarrow v' = 0$, (b) $v = 0 \rightarrow v' = 1$, and (c) $v = 0 \rightarrow v' = 2$ excitations for three approaches $\gamma = 0^\circ, 45^\circ$ and 90° . As reflected from the strengths of VCMEs (Figure 4) the

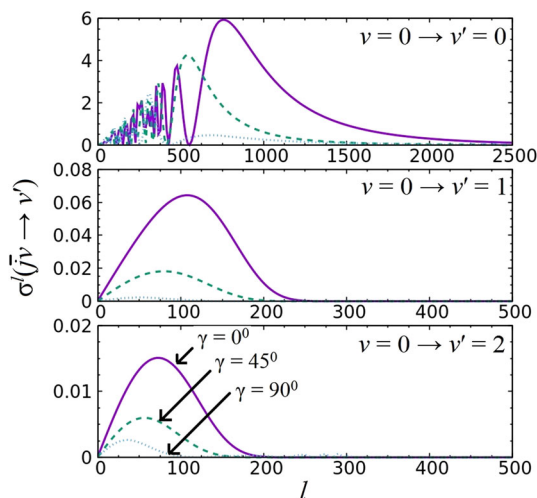


Figure 5. Opacity (partial cross section) as defined in eq. (14) as a function of contributing orbital angular momentum l (in the units of \hbar) for (a) elastic channel, $v = 0 \rightarrow v' = 0$ and inelastic channels (b) $v = 0 \rightarrow v' = 1$ and (c) $v = 0 \rightarrow v' = 2$ for $\gamma = 0^\circ$ (—), 45° (---) and 90° (···).

relative magnitudes of opacities also follow the same order for these orientations. The opacities for elastic channel show lots of oscillations at lower l values. These oscillations successively grow large in magnitude exhibiting finally a large decaying tail which originates from the long-range interaction potential. Their magnitudes are much stronger (approximately by two orders) than those of vibrationally inelastic channels. The magnitudes of the opacities for $v' = 1$ and $v' = 2$ excitations are very small and they follow the order $v' = 1 > v' = 2$, supporting the experimental observations of Böttner *et al.*³

A meaningful comparison between the theory and the experiment involves the comparison of the state-to-state DCSs since they depend critically on both the quality of interaction potential and the accuracy and applicability of the involved theoretical method in their calculations. The total DCS is compared with that of experiment at $E_{c.m.} = 3.64$ eV in Figure 6. The total DCS was obtained after summing up all the rotationally-summed vibrational excitations DCS including rotationally-summed DCS for the elastic channel. Since the experimental DCS was reported in arbitrary units they were normalized with respect to the calculated DCS values at the datum point, $\theta_{c.m.} \approx 36^\circ$. The experimental total DCS shows almost an exponential decay as a function of $\theta_{c.m.}$. Interestingly, there does not appear any signs of a strong rainbow maxima. However, there appears to be a weak and broad rainbow for $\theta_{c.m.}$ in the range, $30^\circ < \theta_{c.m.} < 60^\circ$. The absence of a strong rainbow maximum could

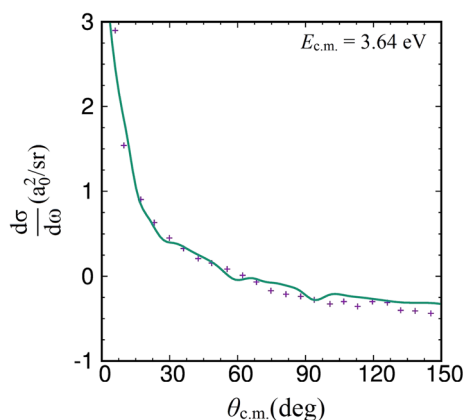


Figure 6. Total DCS as a function of $\theta_{c.m.}$. The present calculations are shown as solid line. The experimental data of Böttner *et al.*,³ are retrieved for comparison, and normalized to the datum point, $\theta_{c.m.} = 36^\circ$. See the text. The number on the ordinate denotes the power of 10.

be attributed to the interference (quenching) effect originating from the inelastic processes. It is gratifying to note that the present VCC-RIOSAs calculations for the total DCS are in quantitative agreement with the experimental data over the entire range of $\theta_{c.m.}$.

The rotationally-summed state-to-state DCS for vibrational excitations are shown in Figure 7. One can see that the magnitude for $v' = 0$ is the largest followed by $v' = 1$ and the magnitudes for $v' = 2$ and $v' = 3$ are extremely small except for ‘hard-hit’ collisions resulting in large angle scattering. This confirms indirectly the experimental observations of Böttner *et al.*,³ that vibrational excitation with $v' = 2$ was very small and $v' = 3$ and above no excitation peaks were observed. Interestingly, all the vibrational inelastic channels exhibit a decreasing trend for $\theta_{c.m.} = 5^\circ$ – 30° and after reaching a minimum around $\theta_{c.m.} \approx 20^\circ$ they increase monotonically with $\theta_{c.m.}$. The elastic $v' = 0$ DCS shows almost an exponential-like decay as a function of $\theta_{c.m.}$. The values of integral cross sections at $E_{c.m.} = 3.64$ eV (in a.u.) for $v' = 0, 1, 2$ and 3 excitations were 439.71, 0.5528, 0.06672 and 0.00707, respectively.

Another striking finding of experiments of Böttner *et al.*,³ is the observation of a large number of rotational excitations in the system which were reflected from the analysis of energy-loss spectra at $E_{c.m.} = 4.23$ eV and $E_{c.m.} = 7.07$ eV at $\theta_{LAB} = 30^\circ, 35^\circ$ and 40° . It was observed that at $E_{c.m.} = 4.23$ eV rotational levels (j') up to 50 could be populated in the vibrational manifold $v = 0$. With the increase in collision energy the magnitude of vibrational excitation $v' = 1$ also increases

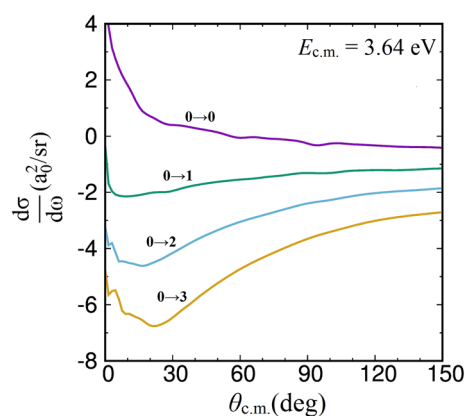


Figure 7. Rotationally summed state-to-state DCS for (i) elastic, $v = 0 \rightarrow v' = 0$ and (ii) inelastic, $v = 0 \rightarrow v' = 1$, $v = 0 \rightarrow v' = 2$ and $v = 0 \rightarrow v' = 3$ channels. The number on the ordinate denotes the power of 10.

and $v' = 1$ manifold also exhibits rotational population up to $j' = 40$. Rotational excitations distribution was reported where $j' \approx 20$ peaked with the maximum magnitude.

As a preliminary examination to this observation we carried out a coupled-state³⁸ study at $E_{c.m.} = 2.47$ eV considering N_2 as a rigid-rotor with $j_i = 0$ using MOLSCAT code.³⁹ The $r = r_{eq}$ value taken as the average value in the ground vibrational state and the rigid-rotor potential was taken as the potential averaged over the ground vibrational state, that is, $V(R, \gamma) = \langle \phi_{v=0}(r) | V(R, r, \gamma) | \phi_{v=0}(r) \rangle$. At this collision energy, transitions up to $j' = 100$ were allowed energetically (open channels). In order to get cross-sections numerically converged for $j' = 50$, additional 20 closed rotational channels were added, and coupled equations were integrated up to the asymptotic limit, $R = 100a_0$ using the log-derivative method. The obtained integral cross sections (up to $j' = 50$) are shown in Figure 8 as solid line. From the calculated values of integral cross-sections (ICSs), we observe that rotational excitations to higher states up to $j' = 50$ are possible but their magnitudes successively decrease with the increase in j' .

While the energy sudden approximation is expected to be still valid in view of large density of rotational states and their small energy separations, it would be worthwhile to incorporate the vibrational–rotational coupling and carrying out coupled-state calculations. To this end, we have carried out vibrational–rotational coupled-state calculations at $E_{c.m.} = 2.47$ eV involving the $v = 0$ and $v = 1$ vibrational levels. We did not include higher vibrational states in view of negligible excitations for $v \geq 2$ as observed in the present calculations and also in the experiments. We kept the rotational

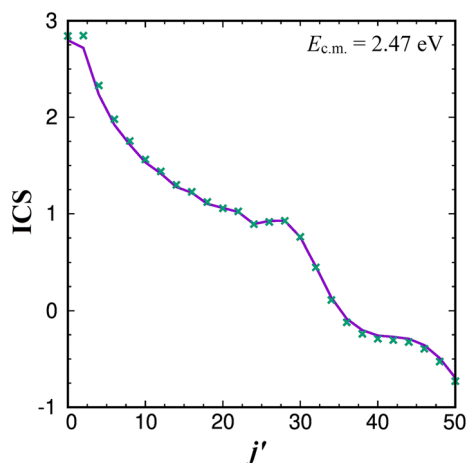


Figure 8. State-to-state integral cross sections (in a.u.) of rotational excitations of N_2 , $v_i = 0$, $j_i = 0 \rightarrow v' = 0$, j' (up to 50) upon collisions of Li^+ at $E_{c.m.} = 2.47$ eV obtained from coupled-state calculations. (x): vib-rotor calculations; (—): rigid-rotor calculations. The number on the ordinate indicates the power of 10.

basis same, that is, j_{max} in $v = 0$ and $v = 1$ manifold was 120. The computed cross sections values for rotational excitations in $v = 0$ are shown in Figure 8 as crosses. The vibrational–rotational coupled-state calculations give similar results for $j' > 6$ in $v = 0$ manifold and for $j' = 2, 4$ the cross sections are marginally higher than those obtained from the RR coupled-state calculations. This suggests that vibrational–rotational coupling increases the magnitudes of rotational excitations for lower j' (up to $j' = 6$). However, for higher j' transitions ($j' > 6$) both the RR and vibrational–rotational coupled-state calculations yield similar results. The magnitudes of integral cross sections of rotational excitations from $v = 0$, $j = 0$ to $v = 1$, j' (with j' up to 50) are very small and all of them have almost the same magnitude suggesting that excitations to all of them are equally probable. Both the vibrational, rotational excitations in $v' = 1$ level are very small as seen in experiments.

Experiments³ reported the rotational excitation distribution at $\theta_{c.m.} = 37.1^\circ, 43.2^\circ$ and 49.2° only for $E_{c.m.} = 4.23$ eV and 7.07 eV. However, it is worthwhile to examine the rotational excitation distribution for the same angles at $E_{c.m.} = 2.47$ eV. Since both RR and vibrational–rotational coupled-state calculations give identical results for $j' > 4$ we analyzed the DCS obtained only from the RR calculations at $E_{c.m.} = 2.47$ eV. We have plotted them in Figure 9. One can see that rotational excitations can occur up to $j' = 20$ with $j' \approx 10$ with maximum magnitude.

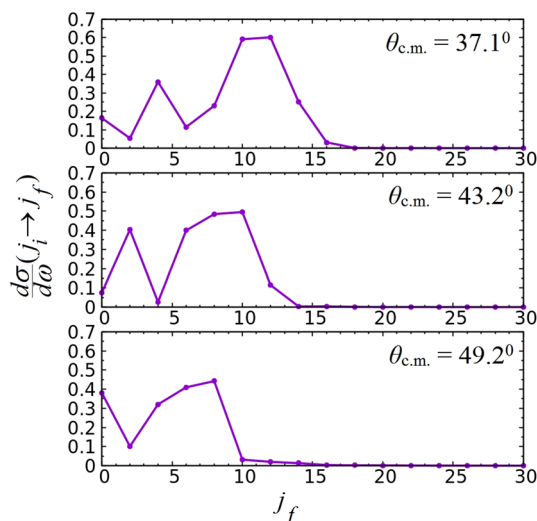


Figure 9. Rotational distributions (j' of N_2) with $j_i = 0$ obtained from the rigid-rotor coupled-state calculations at $E_{c.m.} = 2.47$ eV for $\theta_{c.m.} = 37.1^\circ, 43.2^\circ$ and 49.2° . See the text.

4. Conclusions

In the present study, a new ground electronic state PES of $Li^+ + N_2$ system at the MRCI/aug-cc-pVQZ level of accuracy has been reported in the Jacobi scattering coordinates along with its analytical fit. The long-range interaction has been modelled in terms of charge-quadrupole and polarizability interactions. Various structural characteristics and electronic parameters have been analyzed in detail and they are found to be in good agreement with those available from the experiments as well as earlier theoretical results.

Quantum scattering dynamics study for vibrational excitations has been carried out within VCC-RIOSAs approximation at $E_{c.m.} = 3.64$ eV and various collision attributes have been analyzed in detail. The computed total DCS at $E_{c.m.} = 3.64$ eV is found in quantitative agreement with those of experiments, thus lending credence to the accuracy of the PES.

A preliminary coupled-state study of rotational excitations within the rigid rotor approximation (in $v = 0$ vibrational manifold) is also carried out to examine the potential anisotropy and amount of rotational excitations at $E_{c.m.} = 2.47$ eV. The effect of vibrational–rotational coupling is also examined by carrying out vibrational–rotational coupled-state calculations at $E_{c.m.} = 2.47$ eV. The computed ICSs in both the calculations indicate large number of rotational excitations with appreciable and comparable magnitudes of cross sections for j' up to 50. An analysis of the rotational distribution

at $\theta_{c.m.} = 37.1^\circ$, 43.2° and 49.2° suggests a wide distribution of j' with a maximum around $j' \approx 10$ at this collision energy.

Acknowledgements

We acknowledge the generous computational facility of P. G. Senapathy Computer Center, IIT Madras. A K gratefully thanks the CSIR, New Delhi and IIT Madras for the scholarship.

References

- Faubel M and Toennies J P 1978 Scattering studies of rotational and vibrational excitation of molecules *Adv. At. Mol. Phys.* **13** 229
- Niedner-Schatteburg G and Toennies J P 1992 Proton loss spectroscopy as a state-to-state probe of molecular dynamics *Adv. Chem. Phys.* **82** 553
- Böttner T, Ross U and Toennies J P 1976 Measurements of rotational and vibrational quantum transition probabilities in the scattering of Li^+ from N_2 and CO at center of mass energies of 4.23 and 7.07 eV *J. Chem. Phys.* **65** 733
- Kalugina Y, Lique F and Marinakis S 2014 New ab initio potential energy surface for the rovibrational excitation of $\text{OH}(X^2\Pi)$ by He *Phys. Chem. Chem. Phys.* **16** 13500
- Kohguchi H, Suzuki T and Alexander M H 2001 Fully state-resolved differential cross sections for the inelastic scattering of the open-shell NO molecule by Ar *Science* **294** 832
- Brouard M, Chadwick H, Eyles C J, Hornung B, Nichols B, Scott J M, Aoiz F J, Kols J, Stolte S and Zhang X 2013 The fully quantum state-resolved inelastic scattering of $\text{NO}(X) + \text{Ne}$: experiment and theory *Mol. Phys.* **111** 1759
- Eastes W, Ross U and Toennies J P 1979 Experimental observation of structure in the distribution of final rotational states in small angle inelastic scattering of Li^+ from CO ($E_{c.m.} = 4\text{--}7$ eV) *Chem. Phys.* **39** 407
- Gierz U, Toennies J P and Wilde M 1984 A new look at rotational and vibrational excitation in the scattering of Li^+ from N_2 and CO at energies between 4 and 17 eV *Chem. Phys. Lett.* **110** 115
- Tanuma H, Kita S, Kusunoki I and Sato Y 1989 Observation of site-specific electronic excitation in $\text{Li}^+ - \text{CO}$ collisions near threshold *Chem. Phys. Lett.* **159** 442
- Kita S, Tanuma H, Kusunoki I, Sato Y and Shimakura N 1990 Electronic excitation in moderate-energy $\text{Li}^+ - \text{N}_2$ and $\text{Li}^+ - \text{CO}$ collisions *Phys. Rev. A* **42** 367
- Gisalson E A, Polak-Dingels P and Rajan M S 1990 Determination of the spherically symmetric potential components for $\text{Li}^+ - \text{N}_2$ and $\text{Li}^+ - \text{CO}$ from total cross section measurements *J. Chem. Phys.* **93** 2476 and references therein
- Stammmler V 1975 *Ab initio* calculation of the potential energy surface of the system N_2Li^+ *Chem. Phys.* **7** 17
- Thomas L D 1977 Classical trajectory study of differential cross sections for $\text{Li}^+ - \text{CO}$ and N_2 inelastic collisions *J. Chem. Phys.* **67** 5224
- Poppe B and Böttner D 1978 Inelastic collisions of Li^+ with N_2 molecules: A comparison of experimental results with trajectory studies *Chem. Phys.* **30** 375
- Billing G D 1979 Semiclassical calculations of differential cross sections for rotational/vibrational transitions in $\text{Li}^+ + \text{N}_2$ *Chem. Phys.* **36** 127
- Pfeffer G A and Secrest D 1983 Rotation-vibration excitation using the infinite order sudden approximation for rotational transitions: $\text{Li}^+ - \text{N}_2$ *J. Chem. Phys.* **78** 3052
- (a) Waldman M and Gordon R G 1979 Generalized electron gas-Drude model theory for ion-molecule forces *J. Chem. Phys.* **71** 1353; (b) Dixon D A, Gole J L and Komornicki A 1988 Lithium and sodium cation affinities of H_2 , N_2 and CO *J. Phys. Chem.* **92** 1378; (c) Del Bene J E, Frisch M J, Raghavachari K, Pople J A and Schleyer P V R 1983 A molecular orbital study of some lithium ion complexes *J. Phys. Chem.* **87** 73; (d) Sauer J and Hobza P 1984 The minimal basis set MINI-1—powerful tool for calculating intermolecular interactions. II. Ionic complexes *Theor. Chim. Acta* **65** 291; (e) Ikuta S 1985 *Ab initio* MO calculations on the stable conformations and their binding energies of the ion-molecule complexes: Ion = H^+ , Li^+ , Na^+ , Be^{2+} , Mg^{2+} , and Ca^{2+} ; Molecule = CO and N_2 *Chem. Phys.* **95** 235; (f) Pinchuk V M 1985 Steric and electronic structure of complexes of Li^+ , Na^+ , K^+ , Be^{2+} , Mg^{2+} and Ca^{2+} ions with N_2 molecule *J. Struct. Chem.* **26** 350; (g) Del Bene J E 1986 Basis set and correlation effects on computed lithium ion affinities of some oxygen and nitrogen gases *J. Comput. Chem.* **7** 259
- Kita S, Noda K and Inouye H 1975 Experimental determination of repulsive potentials between alkali ions (Li^+ , Na^+ and K^+) and N_2 and CO molecules *Chem. Phys.* **7** 156
- Grice S T, Harland P W and Maclagan R G A R 1992 Calculation of the potential energy surface of $\text{Li}^+ - \text{N}_2$ *Chem. Phys.* **165** 73
- Falcetta M F and Siska P E 1998 Theoretical study of ion-molecule potentials for He^+ and Li^+ with N_2 *J. Chem. Phys.* **109** 6615
- Bulanin K M, Bulychev V P and Ryazantsev M N 2008 Theoretical study of structural and energy parameters of the van der Waals complex of the Li^+ cation with the N_2 molecule *Opt. Spectrosc.* **105** 829
- Dunning T H 1989 Gaussian basis sets for use in correlated molecular calculations. I. The atoms boron through neon and hydrogen *J. Chem. Phys.* **90** 1007
- Kendall R A, Dunning T H and Harrison R J 1992 Electron affinities of the first-row atoms revisited. Systematic basis sets and wave functions *J. Chem. Phys.* **96** 6796
- (a) Werner H J and Knowles P J 1985 A second order multiconfiguration SCF procedure with optimum convergence *J. Chem. Phys.* **82** 5053; (b) Knowles P J and Werner H J 1985 An efficient second-order MC SCF method for long configuration expansions *Chem. Phys. Lett.* **115** 259
- (a) Werner H J and Knowles P J 1988 An efficient internally contracted multiconfiguration-reference configuration interaction method *J. Chem. Phys.* **89** 5803; (b) Knowles P J and Werner H J 1988 An efficient method for the evaluation of coupling coefficients in configuration interaction calculations *Chem. Phys. Lett.* **145** 514;

- (c) Knowles P J and Werner H J 1992 Internally contracted multiconfiguration-reference configuration interaction calculations for excited states *Theor. Chim. Acta* **84** 95
26. Werner H J, Knowles P J, Knizia G, Manby F R, Schütz M and others, *MOLPRO version 2010.1, a package of ab initio programs*
27. Cade P E, Sales K D and Wahl A C 2004 Electronic structure of diatomic molecules. III. A. Hartree-Fock wavefunctions and energy quantities for $N_2(X_{\Sigma_g^+}^1)$ and $N_2^+(X_{\Sigma_g^+}^2, A_{\Pi_u}^2, B_{\Sigma_u}^2)$ molecular ions *J. Chem. Phys.* **44** 1973
28. Hout J and Bose T K 1991 Determination of the quadrupole moment of nitrogen from the dielectric second virial coefficient *J. Chem. Phys.* **94** 3849
29. Mason E A and McDaniel E W 1988 *Transport Properties of Ions in Gases* (New York: Wiley-Interscience) p. 533
30. Frisch M J, Trucks G W, Schlegel H B, Scuseria G E, Robb M A, Cheeseman J R, Scalmani G, Barone V, Petersson G A, Nakatsuji H, Li X, Caricato M, Marenich A, Bloino J, Janesko B G, Gomperts R, Mennucci B, Hratchian H P, Ortiz J V, Izmaylov A F, Sonnenberg J L, Williams-Young D, Ding F, Lipparini F, Egidi F, Goings J, Peng B, Petrone A, Henderson T, Ranasinghe D, Zakrzewski V G, Gao J, Rega N, Zheng G, Liang W, Hada M, Ehara M, Toyota K, Fukuda R, Hasegawa J, Ishida M, Nakajima T, Honda Y, Kitao O, Nakai H, Vreven T, Throssell K, Montgomery J A, Peralta J E, Ogliaro F, Bearpark M, Heyd J J, Brothers E, Kudin K N, Staroverov V N, Keith T, Kobayashi R, Normand J, Raghavachari K, Rendell A, Burant J C, Iyengar S S, Tomasi J, Cossi M, Millam J M, Klene M, Adamo C, Cammi R, Ochterski J W, Martin R L, Morokuma K, Farkas O, Foresman J B and Fox D J 2016 *Gaussian09, Gaussian, Inc., Wallingford CT*
31. Boys S F and Bernardi F 1970 The calculation of small molecular interactions by the differences of separate total energies. Some procedures with reduced errors *Mol. Phys.* **19** 553
32. Dhillip Kumar T J and Kumar S 2004 Vibrationally inelastic collisions in $H^+ + CO$ system: Comparing quantum calculations with experiments *J. Chem. Phys.* **121** 191
33. Le Roy R J 1996 University of Waterloo Chemical Physics Research Report, Report CP-55R
34. Parker G A and Pack R T 1978 Rotationally and vibrationally inelastic scattering in the rotational IOS approximation. Ultrasimple calculation of total (differential, integral and transport) cross sections for nonspherical molecules *J. Chem. Phys.* **68** 1585
35. Schinke R and McGuire P 1978 Combined rotationally sudden and vibrationally exact quantum treatment of proton- H_2 collisions *Chem. Phys.* **31** 391
36. Gianturco F A 1979 *The transfer of molecular energies by collision* (Berlin: Springer)
37. McGuire P 1976 Coupled states approximation study of inelastic $H^+ - H_2$ collisions at 3.7 eV *J. Chem. Phys.* **65** 3275
38. McGuire P and Kouri D J 1974 Quantum mechanical close coupling approach to molecular collisions. j_z -conserving coupled states approximation *J. Chem. Phys.* **60** 2488
39. Hutson J M and Green S 1994 MOLSCAT computer code, version 14, distributed by the collaborative computational project no. 6 (CCP6) of the Engineering and Physical Sciences Research Council (UK)